Low-Dose Anti-Angiogenic Therapy Sensitizes Breast Cancer to PD-1 Blockade

Qian Li[1,2], Yifan Wang[3], Weijuan Jia[1,2], Heran Deng[1,2], Guangdi Li[4], Weiye Deng[3], Jiewen Chen[1,2], Betty Y.S. Kim[5], Wen Jiang[3], Qiang Liu[1,2], and Jieqiong Liu[1,2]

ABSTRACT

Purpose: Despite its enormous successes, the overall response rate of cancer immunotherapy remains suboptimal, especially in breast cancer. There is an increased interest in combining immune checkpoint inhibitor with targeted agents to enhance antitumor effect. Anti-angiogenic drugs have been shown to synergize with immune checkpoint blockades, but the optimal setting for combining these two modalities and the underlying mechanisms of synergistic responses are not fully understood.

Experimental Design: We tested the combination of anti–PD-1 and different doses of VEGFR2-targeting agents in syngeneic breast cancer mouse models. Tumor-infiltrated immune cell subsets were profiled by flow cytometry. A cytokine array was carried out to identify inflammatory changes in different treatment conditions. The efficacy of combined anti-angiogenic and anti–PD-1 therapy was further evaluated in patients with advanced triple-negative breast cancer (TNBC).

Results: Blockade of VEGFR2 sensitizes breast tumors to PD-1 blockade in a dose-dependent manner. Although both conventional and low-dose anti-VEGFR2 antibody treatments normalize tumor vessels, low-dose VEGFR2 blockade results in more robust immune cell infiltration and activation and promotes the secretion of osteopontin (OPN) by $CD8^+$ T cells. OPN subsequently induces tumor cell production of TGF-β, which in turn upregulates PD-1 expression on immune cells. In patients with advanced TNBC, combined treatment with low-dose anti-VEGFR2 inhibitor and anti–PD-1 demonstrated excellent tolerability and efficacy. Higher OPN and TGF-β expressions correlated with improved treatment responses.

Conclusions: Together, these results demonstrate a dose-dependent synergism between anti-angiogenic therapy and immune checkpoint blockade, thus providing important insights into the optimal strategies for combining immunotherapy with molecular-targeted agents.

Introduction

Cancer immunotherapy employing immune checkpoint inhibitors has resulted in drastic improvements in clinical outcomes in multiple malignant tumors. However, certain poorly immunogenic tumors, such as breast cancer, have intrinsically low-response rates to immunotherapy due to a paucity of tumor-infiltrating T lymphocytes and an abundance of immunosuppressive myeloid cell populations within the tumor microenvironment. Even for triple-negative breast cancer (TNBC), which is more immune sensitive, the objective response rate (ORR) of PD-1/PD-L1 blockade monotherapy from early-phase trials is only 5.2% to 18.5% (1–3). Therefore, there is an increased interest in identifying combination treatment strategies to improve the response rate and the efficacy of immunotherapy treatment (4). The responsiveness of a certain tumor to immune checkpoint inhibitors is likely to depend on multiple tumor intrinsic and extrinsic factors. Among them, the tumor blood vessel plays a critical role (5). Blood vessels within solid tumors are often morphologically abnormal and functionally impaired, resulting in reduced infiltration of immune effector cells into the tumor (5, 6). In addition, tumor blood vessels have impaired perfusion capacity, which creates increased intratumoral hypoxia that inhibits the activity of infiltrated cytotoxic T cells (6) and promotes the accumulation of suppressive immune cells such as myeloid-derived suppressor cells (MDSC) and regulatory T cells (Treg; ref. 7). The hypoxic tumor microenvironment also stimulates the secretion of several immunosuppressive cytokines (8) and promotes the upregulation of PD-1 on T cells (9, 10). Normalization of tumor vasculature has been proposed to reduce immunosuppression and synergize with cancer immunotherapy (11, 12). However, due to the transient and dynamic nature of the process, optimizing vascular normalization to maximize the effect of immune checkpoint inhibitors remains challenging. Previous studies have shown that the immune-stimulating effect and toxicity profiles of anti-angiogenic therapy are highly dependent on its dose and administration schedule (13–15). Therefore, our goal for the present study is to evaluate the optimal conditions for combining anti-angiogenic therapy with an anti–PD-1 agent in syngeneic breast cancer mouse models, and to analyze the efficacy of this treatment strategy in patients with advanced TNBC.

Materials and Methods

Cell lines and reagents

The 4T1 and EMT-6 breast cancer cell lines were obtained from the ATCC and cultured according to the recommended protocols. $CD45^+$

[1]Guangdong Provincial Key Laboratory of Malignant Tumor Epigenetics and Gene Regulation, Sun Yat-sen Memorial Hospital, Sun Yat-sen University, Guangzhou, China. [2]Breast Tumor Center, Sun Yat-sen Memorial Hospital, Sun Yat-sen University, Guangzhou, China. [3]Department of Radiation Oncology, The University of Texas Southwestern Medical Center, Dallas, Texas. [4]Department of Public Health, Central South University, Changsha, China. [5]Department of Neurosurgery, The University of Texas MD Anderson Cancer Center, Houston, Texas.

Note: Supplementary data for this article are available at Clinical Cancer Research Online (http://clincancerres.aacrjournals.org/).

Q. Li, Y. Wang, W. Jia, and H. Deng contributed equally to this article.

Corresponding Authors: Jieqiong Liu, Sun Yat-sen Memorial Hospital, Guangzhou, Guangdong 510120, China. Phone: 86-020-3407-0091; E-mail: liujieqiong01@163.com or liujq7@mail.sysu.edu.cn; Qiang Liu, victorlq@hotmail.com; and Wen Jiang, wen.jiang@utsouthwestern.edu

Clin Cancer Res 2020;26:1712–24

doi: 10.1158/1078-0432.CCR-19-2179

Translational Relevance

Our study demonstrates a dose-dependent synergy between anti-angiogenic therapy and anti–PD-1 antibody in preclinical breast cancer models and in patients with advanced triple-negative breast cancer. We provide compelling evidence that low-dose anti-VEGFR2 therapy is more effective in sensitizing breast cancer to anti–PD-1 therapy through initiation of cytokine crosstalk between osteopontin (OPN) and TGF-β to reprogram the tumor immune microenvironment. Together, these results provide crucial preclinical and clinical insights into an optimized strategy for combining anti-angiogenic therapy and immunotherapy for advanced breast cancer treatment and highlight the important role of OPN in the remodeling of the tumor immune microenvironment. Future studies on OPN as a prognostic biomarker or a potential target for cancer immunotherapy is warranted.

immune cells, $CD8^+$ T cells, $CD4^+$ T cells, $F4/80^+$ macrophages, $CD19^+$ B cells, and $EPCAM^+$ tumor cells, which were sorted out from 4T1, MMTV-PyMT, or EMT-6 models, were cultured in DMEM with 10% FBS. Tumor-infiltrating $CD45^+$ immune cells and primary tumor cells were treated with OPN or progranulin. $CD45^+$ immune cells, $CD8^+$ T cells, $CD4^+$ T cells, $F4/80^+$ macrophages, and $CD19^+$ B cells were treated with 5 ng/mL TGF-β1 for 30 hours.

Cytokine array kit analysis

Tumor-infiltrating $CD45^+$ immune cells were obtained from 4T1 models through fluorescence-activated cell sorting by BD FACSAria III. Then, they were cultured in DMEM supplemented with 10% FBS at 37°C in 24-well culture plates for 48 hours. The supernatant of cultured cells was collected and sent to Raybiotech (Guangzhou, China) for cytokine analysis (mouse cytokine array kit GS2000). Reagents were supplied with the array kit, and all experiments were performed according to the manufacturer's instructions. The data were collected and analyzed by Raybiotech.

ELISA

Osteopontin (OPN) ELISA kits and progranulin ELISA kits were purchased from Raybiotech, and TGF-β ELISA kits were purchased from Boster. All experiments were performed according to the manufacturer's instructions.

Western blot

For protein extraction, tumor cells and tumor-infiltrating immune cells were homogenized by Ripa (Millipore) with a proteinase inhibitor cocktail. Total protein was quantified using the Pierce BCA Protein Assay Kit. Equal amounts of the lysates were separated by 10% SDS-PAGE and electro-transferred to nitrocellulose membranes (Whatman Protran nitrocellulose membrane; neoLab). After being blocked with TBS/0.05% Tween-20/5% skim milk, the membranes were probed with antibodies against PD-1 or GAPDH. Peroxidase-conjugated anti-rabbit antibody was used as secondary antibodies, and signals were captured by chemiluminescence (ECL; Thermo Fisher). Specific information on antibodies is listed in Supplementary Table S1.

Animal studies

All animal studies were reviewed and approved by the Institutional Animal Care and Use Committee of Sun Yat-sen University. For 4T1 and EMT-6 BC experiments, BALB/c Mice were anaesthetized, and 2×10^5 cells (4T1 model) or 5×10^5 cells (EMT-6 model) were injected directly into the mammary fat pad. For MMTV-PyMT experiments, we directly implanted the syngeneic MMTV-PyMT breast cancer tumor blocks (1 mm^3) into the mammary fat pad of female FVB/n mice of 4 to 5 weeks of age. When tumors reached a volume of 20 mm^3, mice bearing 4T1 or MMTV-PyMT tumors were randomized to receive one of the following treatments by intraperitoneal injection (twice a week for 2 weeks): rat IgG2a (40 mg/kg), anti–PD-1 antibody (10 mg/kg), full dose of DC101 antibody (anti-VEGFR2, 40 mg/kg), low dose of DC101 (10 mg/kg), full dose of DC101 (40 mg/kg) plus anti–PD-1, or low dose of DC101 (10 mg/kg) plus anti–PD-1. Moreover, mice bearing 4T1 or EMT-6 tumors received one of the following treatments: rat IgG2a (40 mg/kg), anti–PD-1 antibody (10 mg/kg), full dose of apatinib (150 mg/kg), low dose of apatinib (50 mg/kg), full dose of apatinib (150 mg/kg) plus anti–PD-1, low dose of apatinib (50 mg/kg) plus anti-PD-1, or low dose of DC101 (10 mg/kg) plus anti–PD-1. Tumor growth was monitored every 3 days by measuring tumor length (L) and width (W). Tumor volume (V) was then calculated using the formula, $V = 1/2 \times L \times W^2$. To identify lung metastasis and to analyze survival, we treated mice with drugs (as above) for 7 to 8 weeks, collected the lungs, dissected and washed them, then fixed them in 4% paraformaldehyde for 24 hours. Metastatic lung nodules were counted directly. Specific information on antibodies is listed in Supplementary Table S1. The survival endpoint of tumor-bearing mice was reached when the primary tumor diameter was greater than 20 mm, or when the animal demonstrated signs of severe pain and discomfort, or when the animal died because of disease progression.

Depletion experiments

Mice were injected intraperitoneally with 1 mg of rat IgG1, clodronate liposomes, or anti-CD8 antibody one day before treatment with drugs and then with 0.5 mg every 5 days thereafter. To deplete $CD4^+$ T cells, mice were injected intraperitoneally with 0.4 mg anti-CD4 antibody one day before treatment and then with 0.4 mg every 4 days for the next 2 weeks. To deplete B cells, mice were injected intraperitoneally with 0.1 mg of anti-CD20 antibody once per week. For OPN depletion experiments, mice were treated with 10 μg of mouse OPN antibody (intraperitoneally) every day from day 1 after treatment with DC101 or $DC101^+$ anti–PD-1 drugs. Specific information on antibodies is listed in Supplementary Table S1.

Isolation of primary tumor cells and blood cells from mouse models

Briefly, tumor tissues were exhaustively flushed with PBS, minced into small (1–2 mm in diameter) pieces, and digested with 2% FBS DMEM containing 2 mg/mL collagenase IV (Sigma) at 37°C for 30 minutes. Cells were sequentially filtered through a 500-μm mesh and 100 and 40-μm cell strainers. Then, they were centrifuged in a Beckman Allegra X-15R centrifuge at 2,500 rpm for 15 minutes with 1 mL cell suspension above 5 mL 45% Percoll (GE Healthcare) in the middle and 5 mL 60% Percoll at the bottom in a 15 mL tube. Primary tumor cells were collected from the cell layer in the interface above 45% Percoll and further purified by Cancer Cell Isolation Kit (Panomics). Mononuclear cells were collected from the cell layer at the interface between 45% and 60% Percoll. Mononuclear cells from blood were also isolated by Ficoll density-gradient centrifugation.

Immunohistochemistry and immunofluorescence

Paraffin-embedded samples were cut into 5-μm consecutive sections and deparaffinized. Specimens were incubated at 4°C overnight with antibodies against human OPN, TGF-β1, PD-1, CD8, CD19, or CD68, or against mouse CD8α, CD20, F4/80, or CD4. Specimens were then washed by PBS and stained with anti-mouse/rabbit immunohistochemistry (IHC) secondary antibody kit or incubated with Alexa Fluor secondary antibodies. PD-L1 expression on patient tumor samples was assessed using the FDA-approved 22C3 assay on the Dako Link 48 platform following the manufacturer's instructions (16). The PD-L1 positivity threshold on ICs or TCs was set at ≥1% PD-L1–expressing immune cells or tumor cells as a percentage of the tumor area. Double fluorescent staining with anti-CD31 and anti-NG2 was performed on snap-frozen sections embedded in OCT compound (8 μm), then 5–10 areas per tumor sample were randomly selected for analysis. Specific information on antibodies is listed in Supplementary Table S1.

Flow-cytometric analysis

Single-cell suspensions were prepared. Cells were incubated on ice for 30 minutes with fluorescence-labeled antibodies against PD-L1, PD-1, CD8, CD4, CD19, CD3, F4/80, CD45, granzymeB, IFN-γ, CD69, IgM, CD43, CD5, CD1d, CD11c, MHC-II, TGF-β or OPN. Intracellular cytokine staining was performed using the Intracellular Fixation and Permeabilization kit according to the manufacturer's instructions. After being washed, stained cells were separated on a Beckman CytoFLEX Flow cytometer. Data were analyzed on FlowJo software. Specific information on antibodies is listed in Supplementary Table S1.

Patient samples

All patient-related procedures were performed with the approval of the Internal Review and the Ethics Boards of the Sun Yat-sen Memorial Hospital. Written informed consent was obtained from all patients. The tumor samples were obtained from 12 patients with advanced TNBC who were treated with SHR-1210 (anti–PD-1 antibody, 200 mg for patients whose weight is ≥50 kg or 3 mg/kg for those whose weight is below 50 kg, Q2W, intravenous) combined with low-dose apatinib (250 mg, oral, daily) at the Breast Tumor Center of Sun Yat-Sen Memorial Hospital between January 2018 and July 2019. These patients were part of the apatinib continuous dosing arm of an ongoing phase II, open-label trial (NCT03394287) of SHR-1210 in combination with apatinib (VEGFR2-TKI) in patients with advanced TNBC.

Key eligibility criteria included women ages 18- to 70-years-old with metastatic or unresectable recurrent TNBC; measurable disease per Response Evaluation Criteria in Solid Tumors (RECIST) v1.1; an Eastern Cooperative Oncology Group performance status of 0/1; had received fewer than 3 lines of systemic therapies in the metastatic setting; had adequate organ and bone marrow function; and had a representative tumor sample (paraffin and/or fresh tissue). Tumors were assessed every 8 weeks for the first 24 weeks and every 12 weeks thereafter during treatment. The cutoff date for analyses in the current study was July 31, 2019. Samples of pre-treatment metastatic/recurrent tumor tissues or metastatic/recurrent tissues after 8 weeks of combination therapy were collected by core needle biopsy.

Statistical analysis

A completely randomized, balanced design was used for all experiments. Student *t* test or the Mann–Whitney *U* test were used to test the significance of differences in various molecular, cellular, and physiological parameters between the means or medians in treatment and control groups. A *P* value less than 0.05 was considered significant. Error bars in the experiments indicate standard error of the mean (SEM) or standard deviation (SD) for a minimum of three independent experiments.

Results

Low-dose anti-VEGFR2 antibody improves the antitumoral activity of PD-1 inhibitor in breast carcinoma

We first treated orthotopically implanted 4T1 and MMTV-PyMT mammary breast tumors with anti–PD-1 antibody in combination with murine anti-VEGFR2 antibody, DC101 at different dosing regimen. Both anti–PD-1 antibody and low-dose DC101 (10 mg/kg) as a single agent exhibited limited antitumoral activity. In contrast, the combination of anti–PD-1 antibody and low-dose DC101 significantly inhibited tumor growth and the formation of lung metastases. Interestingly, we noted that low-dose DC101 resulted in a more profound tumor growth inhibitory effect and longer survival than full-dose DC101 when combined with anti–PD-1 in both 4T1 (**Fig. 1A–C**) and MMTV-PyMT tumors (Supplementary Fig. S1A–S1C).

Low-dose anti-VEGFR2 normalizes tumor vessels and increases tumor infiltration of immune effector cells

To investigate the mechanisms underlying the observed dose-dependent responses, we evaluated tumor blood vessel changes after combination treatment. Treatment with full-dose DC101 resulted in a prominent anti-angiogenic effect with a significant degree of vessel regression (**Fig. 1D**; Supplementary Fig. S1D). In contrast, low-dose DC101 therapy increased pericyte coverage and tumor vessel normalization effect (**Fig. 1E**; Supplementary Fig. S1E). Consistent with a prior report (11), we found that anti–PD-1 monotherapy also had a vascular normalization effect, which was further enhanced by DC101 (**Fig. 1E**; Supplementary Fig. S1E).

Given that normalized tumor vessels could not only improve tissue perfusion and reduce intratumoral hypoxia, but may also facilitate the infiltration and activation of immune effector cells within the tumor microenvironment (5, 6, 17), we next evaluated how different doses of DC101 treatment affected the infiltration of intratumoral immune cells. We found that both low- and full-dose DC101 increased the tumor infiltration of $CD8^+$ T cells, macrophages, and B cells (**Fig. 1F**; Supplementary Fig. S2A and S2B), decreased the infiltration of Tregs and MDSCs, but had no effect on the infiltration of $CD4^+$ T cells and regulatory B cells (Supplementary Fig. S2C). However, tumor infiltration of $CD8^+$ T and macrophages was more prominent in tumors treated with low-dose DC101 (**Fig. 1F**; Supplementary Fig. S2A–S2B). We observed similar results in MMTV-PyMT tumors (Supplementary Fig. S2D and S2E). When combined with anti–PD-1 antibody, we also noted increases in the proportion of activated $CD8^+$ T cells and M1-like ($CD11c^+$ $MHC\text{-}II^+$) macrophages, as well as the $CD43^+IgM^{high}$ B1 cells, in tumors treated with low-dose DC101 (**Fig. 1G**; Supplementary Fig. S3A–S3E). Collectively, these results suggest that low-dose anti-VEGFR2 antibody treatment more effectively normalizes tumor blood vessels and increases the tumor infiltration of effector immune cells in breast carcinomas when combined with anti–PD-1 agents.

Antitumor activity of anti-VEGFR2 and anti–PD-1 combination therapy relies on $CD8^+$ T and B lymphocytes

To assess whether the increased infiltration of immune effector cells contributes to the antitumor activities of anti-VEGFR2 and anti-PD-1 agents, we depleted these cell populations (**Fig. 1H**; Supplementary

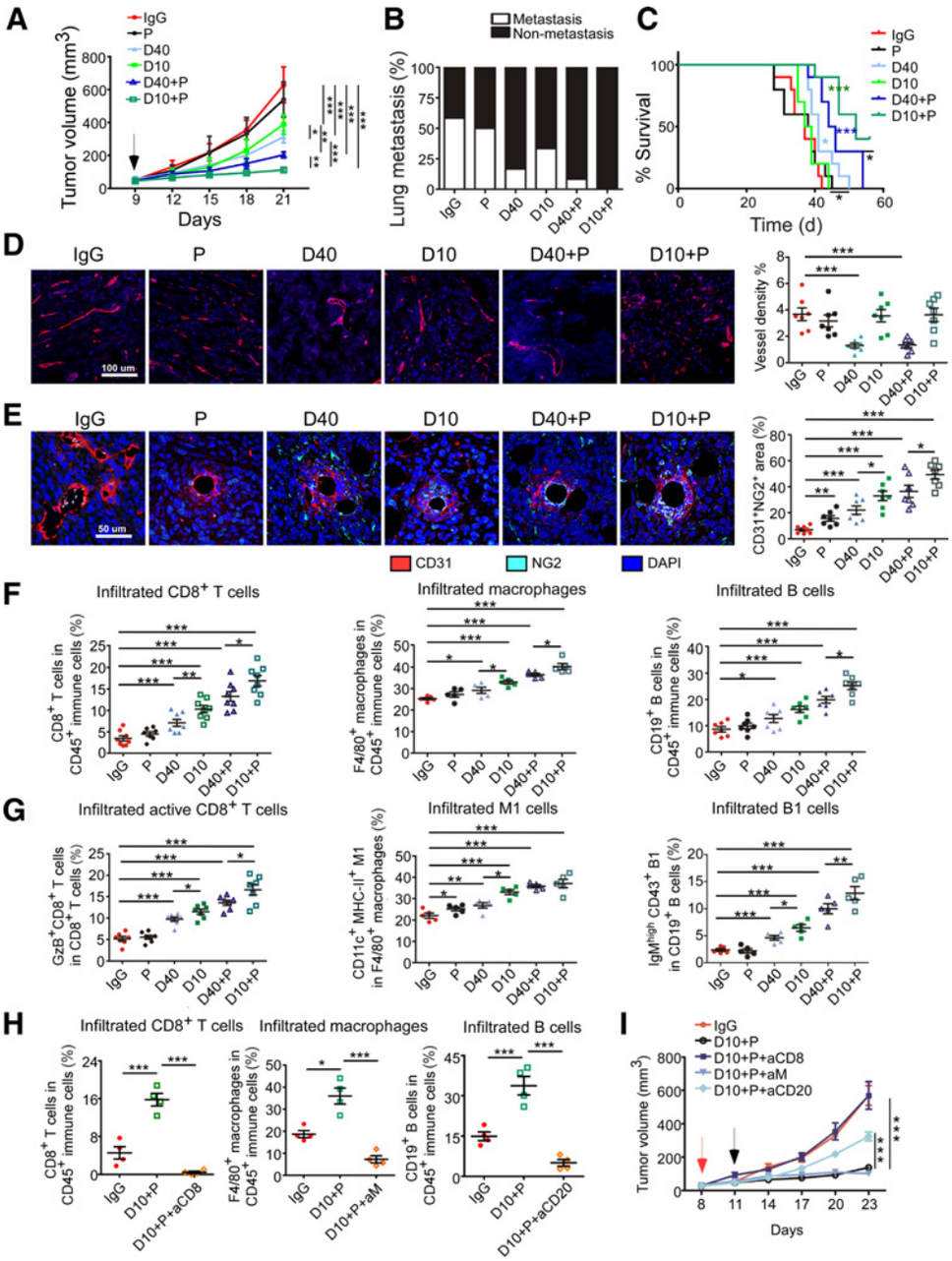

Figure 1.

Low-dose anti-VEGFR2 antibody improved antitumoral activity of anti–PD-1 immune therapy for normalizing tumor blood vessels and more robustly increasing tumor infiltration of $CD8^+$ T cells, macrophages, and B cells in 4T1 models. **A,** Tumor growth curves of 4T1 tumor-bearing mice. The black arrow indicates the start of treatment. Number of experimental mice: IgG, $n = 10$; anti–PD-1, $n = 6$; DC101 10 mg/kg, $n = 8$; DC101 40 mg/kg, $n = 6$; DC101 10 mg/kg + anti–PD-1, $n = 8$; and DC101 40 mg/kg + anti–PD-1, $n = 8$. **B,** Number of metastases in the lungs of 4T1 tumor-bearing mice. Mice were euthanized 9 weeks after tumor injection ($n = 10$ per group). **C,** Survival of the 4T1 tumor-bearing mice treated as indicated since the day of tumor injection ($n = 10$ per group). **D,** Blood vessel density in 4T1 tumors. Representative images of CD31 immunostaining (red) of 4T1 tumors treated as indicated; scale bars, 100 μm. Each dot indicates one tumor per mouse and represents the average of 5–10 images ($n = 7$ per group). **E,** Blood vessel normalization in 4T1 tumors. Representative images of CD31 (red) and NG2 (cyan) immunostaining and DAPI nuclear staining (blue) of 4T1 tumors treated as indicated; scale bars, 50 μm. Each dot indicates one tumor per mouse and represents the average of 5–10 images ($n = 7$ per group). **F,** Flow-cytometry analysis of $CD8^+$ T cells (anti–PD-1, $n = 10$; $n = 7$ per other group), $F4/80^+$ macrophages ($n = 5$ per group), and $CD19^+$ B cells ($n = 5$ per group) in 4T1 tumors. **G,** Flow-cytometry analysis of GzB^+ $CD8^+$ T cells ($n = 7$ per group), $CD11c^+$ MHC-II^+ $F4/80^+$ M1-like macrophages ($n = 5$ per group), and IgM^{high} $CD43^+$ $CD19^+$ b1-like B cells ($n = 5$ per group) in 4T1 tumors. Each dot indicates one tumor per mouse. **H,** Flow cytometry of $CD8^+$ T cells, $CD19^+$ B cells, and $F4/80^+$ macrophages in the tumor microenvironment of mice carrying 4T1 tumors treated as indicated. Each dot represents one mouse. IgG refers to the isotype control for treatment. **I,** Tumor growth curves of 4T1 tumors treated as indicated ($n = 4$ per group). The black arrow indicates the start of treatment, and the red one indicates the start of depletion. Each dot indicates one tumor per mouse. Data are presented as means ± SEM. *, $P < 0.05$; **, $P < 0.01$; ***, $P < 0.001$ by Student t test.

Fig. S4A). Because we did not observe increased $CD4^+$ T-cell infiltration in low-dose DC101-treated 4T1 tumors, we elected not to deplete this cell subset in this model. In both 4T1 and MMTV-PyMT tumors, anti-CD20 or anti-CD8 treatment significantly abrogated the antitumoral effects of low-dose DC101 and anti–PD-1 combination therapy, whereas depletion of macrophages showed no effect on tumor growth (**Fig. 1I**; Supplementary Fig. S4B). These results suggest that $CD8^+$ T cells, B cells, and to a lesser extent, $CD4^+$ T cells play important roles in the antitumoral activity of low-dose anti-VEGFR2 plus anti–PD-1 combination therapy.

Differential upregulation of PD-1/PD-L1 checkpoints by anti-VEGFR2 treatment

Previous studies have reported that tumor-infiltrating $CD8^+$ T cells elicited by full-dose anti-angiogenic therapy upregulate PD-L1 in tumors through interferon-γ (IFN-γ), which may sensitize the tumor to anti–PD-1 therapy (11, 12). Thus, we evaluated whether low-dose DC101 treatment also upregulated PD-L1. We found that PD-L1 expressions on tumor, endothelial, and $CD45^+$ immune cells were elevated during both low-dose and full-dose DC101 treatment in both models (**Fig. 2A**; Supplementary Fig. S5A). Furthermore, we found that DC101 treatment increased IFN-γ^+CD8^+ T cells more than 2-fold in both models (**Fig. 2B**; Supplementary Fig. S5B).

We found that low-dose DC101 improves the antitumoral activity of anti–PD-1 therapy more than full-dose DC101, but this improvement difference between low-dose and full-dose cannot be explained by PD-L1 upregulation during DC101 treatment, so additional mechanisms may be involved. Several clinical studies revealed that intratumoral PD-1 expression on TILs with high PD-1 expression was associated with response following anti–PD-1 blockade (18–20). Therefore, we compared the PD-1 expression in tumor-infiltrating immune cells after low- and full-dose DC101 treatment. We found that PD-1 expressions on $CD45^+$ immune cells, $CD8^+$ T cells, $CD4^+$ T cells, and macrophages were upregulated during low-dose but not full-dose DC101 treatment (**Fig. 2C**; Supplementary Fig. S5C). Furthermore, PD-1 expression was upregulated in B cells during low-dose therapy in 4T1 tumors (**Fig. 2C**), and by both low- and full-dose DC101 in MMTV-PyMT tumors (Supplementary Fig. S5C). Together, these data suggest that, although full- and low-dose DC101 upregulate PD-L1 expression in tumors, low-dose DC101 appeared to be more efficient in upregulating PD-1 expression on tumor-infiltrating immune cells, which may further sensitize the tumor to anti–PD-1 treatment.

Low-dose anti-VEGFR2 antibody-induced PD-1 expression relies on OPN

To determine how low-dose anti-VEGFR2 antibody upregulated PD-1 expression on tumor-infiltrating immune cells, we isolated $CD45^+$ cells from tumors treated with IgG, full-dose, or low-dose DC101 and performed cytokine analysis. We found that, in low-dose DC101-treated tumors, there are 6 cytokines exhibited >4-fold increase than those from full-dose treated tumors (**Fig. 3A**; Supplementary Fig. S6A). Q-PCR and ELISA assays further validated that progranulin and OPN were elevated in the $CD45^+$ immune cells from low-dose DC101-treated tumors (**Fig. 3B**).

We next tested whether progranulin or OPN could induce the upregulation of PD-1 expression on immune cells. Neither progranulin nor OPN was found to directly increase PD-1 expression on $CD45^+$ immune cells isolated from tumors (**Fig. 3C**; Supplementary Fig. S6B). Given that TGF-β1 has been reported to increase PD-1 expression on tumor-infiltrating $CD8^+$ T cells, we tested whether progranulin or OPN could upregulate PD-1 on immune cells indirectly. We found that stimulation of TGF-β1 *in vitro* upregulated PD-1 expression on $CD8^+$ T cells, $CD4^+$ T cells, and macrophages from 4T1 tumors (**Fig. 3D**). Furthermore, OPN treatment induced tumor cells but not $CD45^+$ immune cells to secrete TGF-β1, while progranulin only induced $CD45^+$ immune cells but not tumor cells to secrete TGF-β1 (**Fig. 3E**). Similarly, we found that tumor cells treated with low-dose DC101 *in vivo* expressed more TGF-β1 than those treated with full-dose DC101, but there was no statistical difference in TGF-β1 expression by $CD45^+$ immune cells among different treatment groups (**Fig. 3F** and **G**; Supplementary Fig. S6C). In addition, low-dose DC101 treatment resulted in 2-fold higher TGF-β1 expression in tumor cells than in $CD45^+$ cells (**Fig. 3F**). These results indicate that the TGF-β1 produced by tumors may play a predominant role in PD-1 upregulation on immune cells after low-dose DC101 treatment, likely mediated by OPN-induced TGF-β1 production in tumors.

To validate the role of OPN in the tumor microenvironment, we blocked OPN *in vivo* using a neutralizing antibody. OPN neutralization diminished the synergy between low-dose DC101 and anti–PD-1 treatments (**Fig. 4A**). In addition, TGF-β1 secretion by tumor cells was also downregulated by anti-OPN treatment (**Fig. 4B**). Finally, PD-1 expressions on $CD8^+$ T and $CD19^+$ B cells upon low-dose DC101 treatment were decreased by anti-OPN, whereas PD-1 expressions on $CD4^+$ T cells and $F4/80^+$ macrophages were not altered (**Fig. 4C**). The tumor infiltration of $CD8^+$ T cells, macrophages and B cells was not affected by OPN neutralization (Supplementary Fig. S6D). Therefore, OPN-induced tumor TGF-β secretion functions as the driver for PD-1 upregulation on $CD8^+$ T cells and $CD19^+$ B cells.

We then sought to determine which specific cell populations are mainly responsible for OPN production. We found that low-dose DC101-treated tumors had more OPN^+ $CD8^+$ T cells and OPN^+ macrophages than full-dose DC101-treated tumors, whereas numbers of OPN^+ $CD4^+$ T cells and OPN^+ B cells had no significant differences between these tumors in both models (Supplementary Fig. S6E and S6F). Together, these data suggest that low-dose DC101 induces OPN secretion by $CD8^+$ T cells and macrophages, which then upregulates TGF-β expression in tumor cells. The increased TGF-β subsequently promotes PD-1 expression on immune cells (**Fig. 5**).

PD-1 blockade synergizes with low-dose small-molecule VEGFR2 tyrosine kinase inhibitor in TNBC animal models

Small-molecule anti-angiogenic tyrosine kinase inhibitors (TKI), such as apatinib, have been approved for treating several types of cancer. To investigate whether our findings can be translated to the small-molecule VEGFR2 inhibitor setting, we tested high and low doses of apatinib in combination with anti–PD-1 therapy in 4T1 and EMT-6 TNBC models. Similar to the results with DC101 (**Fig. 1**), low-dose apatinib (50 mg/kg) showed a better antitumor effect than high-dose apatinib (150 mg/kg) when combined with anti–PD-1 (Supplementary Fig. S7A and S7B). Low-dose apatinib normalized tumor blood vessels better than high-dose apatinib (Supplementary Fig. S7C and S7D). The combination of low-dose apatinib increased $CD8^+$ T-cell infiltration more than high-dose (Supplementary Fig. S7E). Similarly, the PD-1 expression on tumor infiltrated $CD45^+$ immune cells was upregulated by low-dose but not high-dose apatinib (Supplementary Fig. S7F). Low-dose apatinib stimulated $CD8^+$ T cells to secrete OPN, an effect not observed after high-dose treatment (Supplementary Fig. S7G). In summary, our data suggest that low-dose anti-angiogenic TKI also synergize with anti–PD-1 better than high-dose.

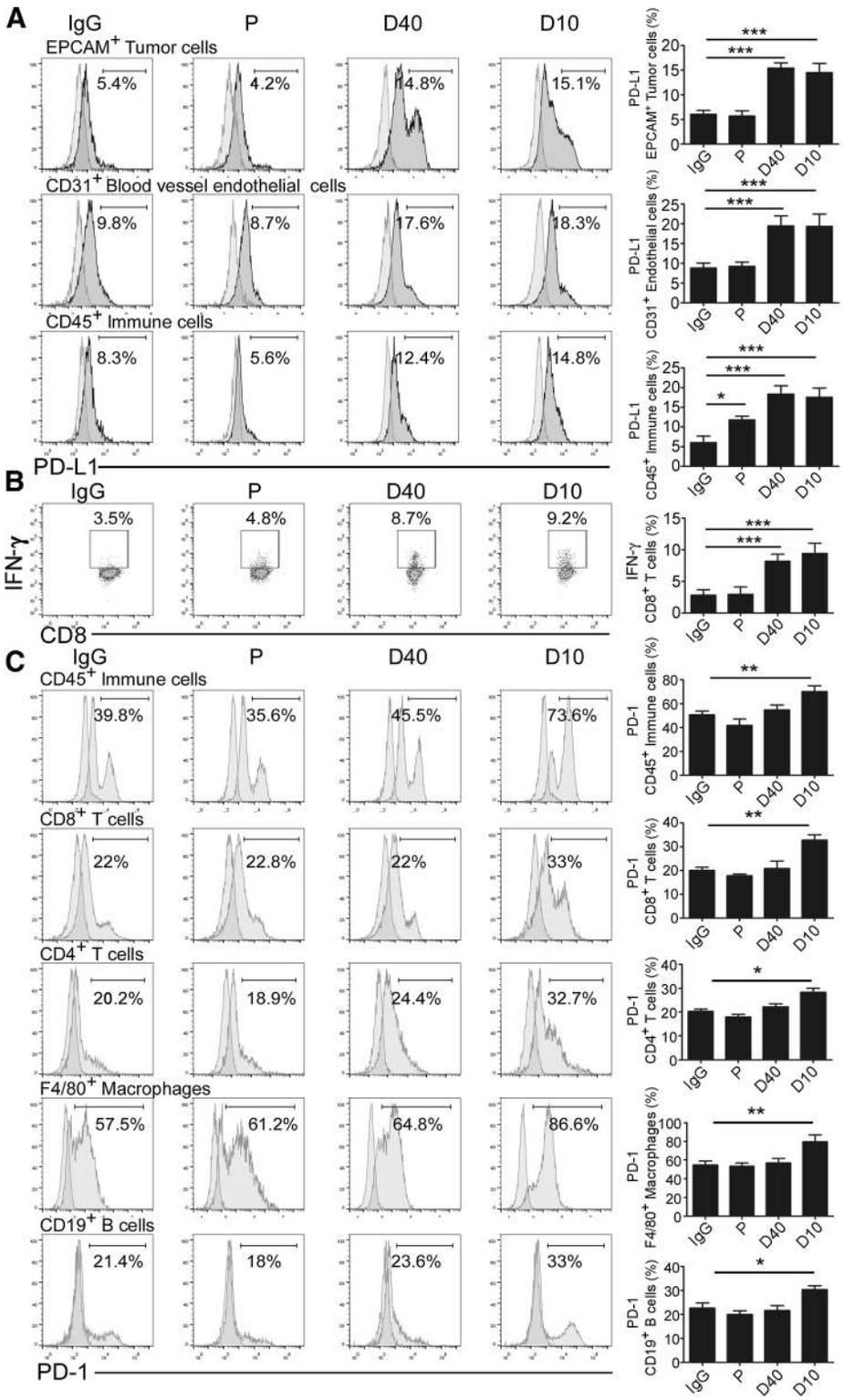

Figure 2.

PD-1 expression on tumor-infiltrating immune cells was upregulated only by low-dose anti-VEGFR2 treatment in 4T1 models. **A,** Flow-cytometry analysis of PD-L1 on EPCAM$^+$ tumor cells, CD31$^+$ blood vessel endothelial cells, and CD45$^+$ immune cells in 4T1 tumors treated as indicated (n = 5 per group). **B,** Flow-cytometry analysis of IFN-γ on CD8$^+$ T cells (n = 5 per group). **C,** Flow cytometry of PD-1 on total CD45$^+$ immune cells (n = 6 per group), CD8$^+$ T cells (n = 6 per group), CD4$^+$ T cells (n = 3 per group), F4/80$^+$ macrophages (n = 6 per group), and CD19$^+$ B cells (n = 5 per group). Data are presented as means ± SEM. *, $P < 0.05$; **, $P < 0.01$; ***, $P < 0.001$ by Student t test.

Combined low-dose VEGFR2 inhibitor and PD-1 blockade exhibits antitumor activities in patients with advanced TNBC

To assess whether low-dose VEGFR2 inhibitor combined with anti–PD-1 antibody can produce clinical antitumor activity in patients with breast cancer, we conducted a phase II, open-label trial of SHR-1210 (anti–PD-1 antibody) in combination with apatinib (VEGFR2-TKI) for advanced TNBC (NCT03394287). Samples of pre-treatment metastatic/recurrent tumor tissues or metastatic/recurrent tissues were

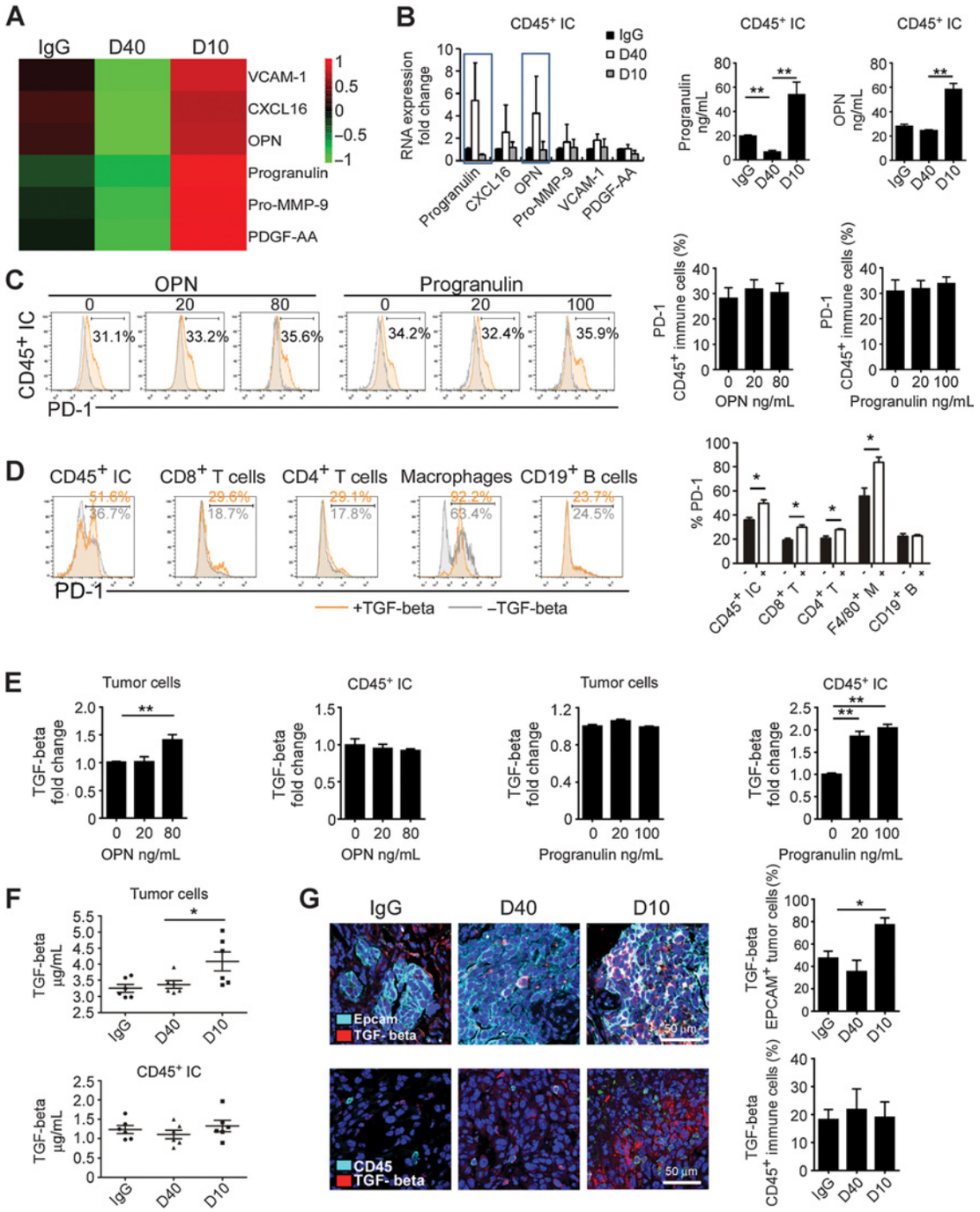

Figure 3.

Low-dose of anti-VEGFR2 antibody upregulated PD-1 expression in tumor-infiltrating immune cells by inducing TGF-β secretion by tumor cells. **A,** Cytokine arrays for condition media of CD45$^+$ immune cells sorted from 4T1 tumors. **B,** The mRNA expression verification for CD45$^+$ immune cells sorted from 4T1 tumors and cytokine protein levels of cell supernatant, which were validated by ELISA ($n = 4$ per group). **C,** Flow-cytometry analysis of PD-1 expression in CD45$^+$ immune cells sorted out from IgG-treated 4T1 tumors and treated with different doses of OPN and progranulin ($n = 4$ per group). **D,** Flow-cytometry analysis of PD-1 expression in CD45$^+$ immune cells, CD8$^+$ T cells, CD4$^+$ T cells, F4/80$^+$ macrophages, and CD19$^+$ B cells after treatment with 5 ng/mL recombinant mouse TGF-β1 for 30 hours ($n = 4$ per group). **E,** ELISA assay of TGF-β1 secretion from the condition media collected from tumor cells and CD45$^+$ immune cells, which were treated with different doses of OPN and progranulin ($n = 4$ per group). **F,** ELISA assay of TGF-β1 secretion from the condition media collected from tumor cells and CD45$^+$ immune cells, which were cultured alone for 48 hours ($n = 6$ per group). **G,** TGF-β1 expression in 4T1 tumors. Representative images of TGF-β1 (red), EPCAM (cyan), and CD45 (cyan) immunostaining, and DAPI nuclear staining (blue) of 4T1 tumors treated as indicated; scale bars, 50 μm. Represents the average of 5–10 images ($n = 4$ per group). Data are presented as means ± SEM. *, $P < 0.05$; **, $P < 0.01$; ***, $P < 0.001$ by Student t test.

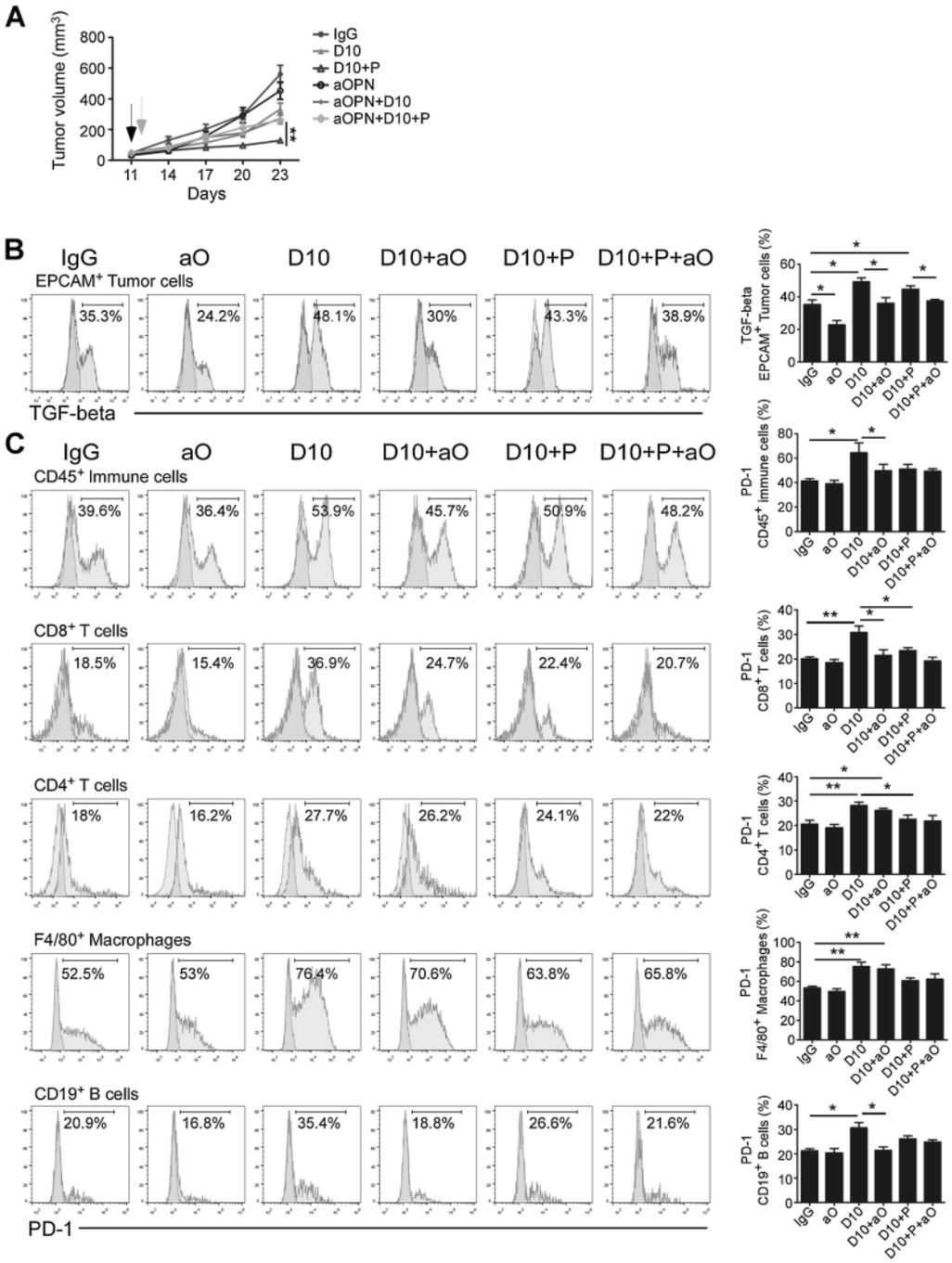

Figure 4.

Blocking of OPN *in vivo* diminished the antitumor effect of anti–PD-1 plus low-dose DC101 combination treatment. **A,** Tumor growth curves of 4T1 tumor-bearing mice treated as indicated ($n = 4$ per group). The black arrow indicates the start of treatment, and the gray one indicates the start of OPN depletion. **B,** Flow-cytometry analysis of TGF-β^+ tumor cells ($n = 4$ per group). **C,** Flow cytometry of PD-1 expression on $CD45^+$ immune cells, $CD8^+$ T cells, $CD4^+$ T cells, $F4/80^+$ macrophages and $CD19^+$ B cells ($n = 4$ per group). Data are presented as means ± SEM. *, $P < 0.05$; **, $P < 0.01$; ***, $P < 0.001$ by Student *t* test.

collected after 8 weeks of combination therapy. At the cutoff date for data analysis of this study, a total of 12 patients were enrolled in the continuous dosing arm and received low-dose apatinib (250 mg/d, half of the recommended 500 mg/d dose for patients with advanced TNBC) combined with SHR-1210 (200 mg/Q2W). Among these patients, 10 (83.3%) had visceral metastasis, and 7 (58.3%) were PD-L1 negative on tumor cells, while 9 (75%) were PD-L1 negative on immune cells. At the time of data analysis, three patients were still on treatment, and two of them had been on treatment for more than one year. The minimum follow-up time for these patients was 3 months. The median

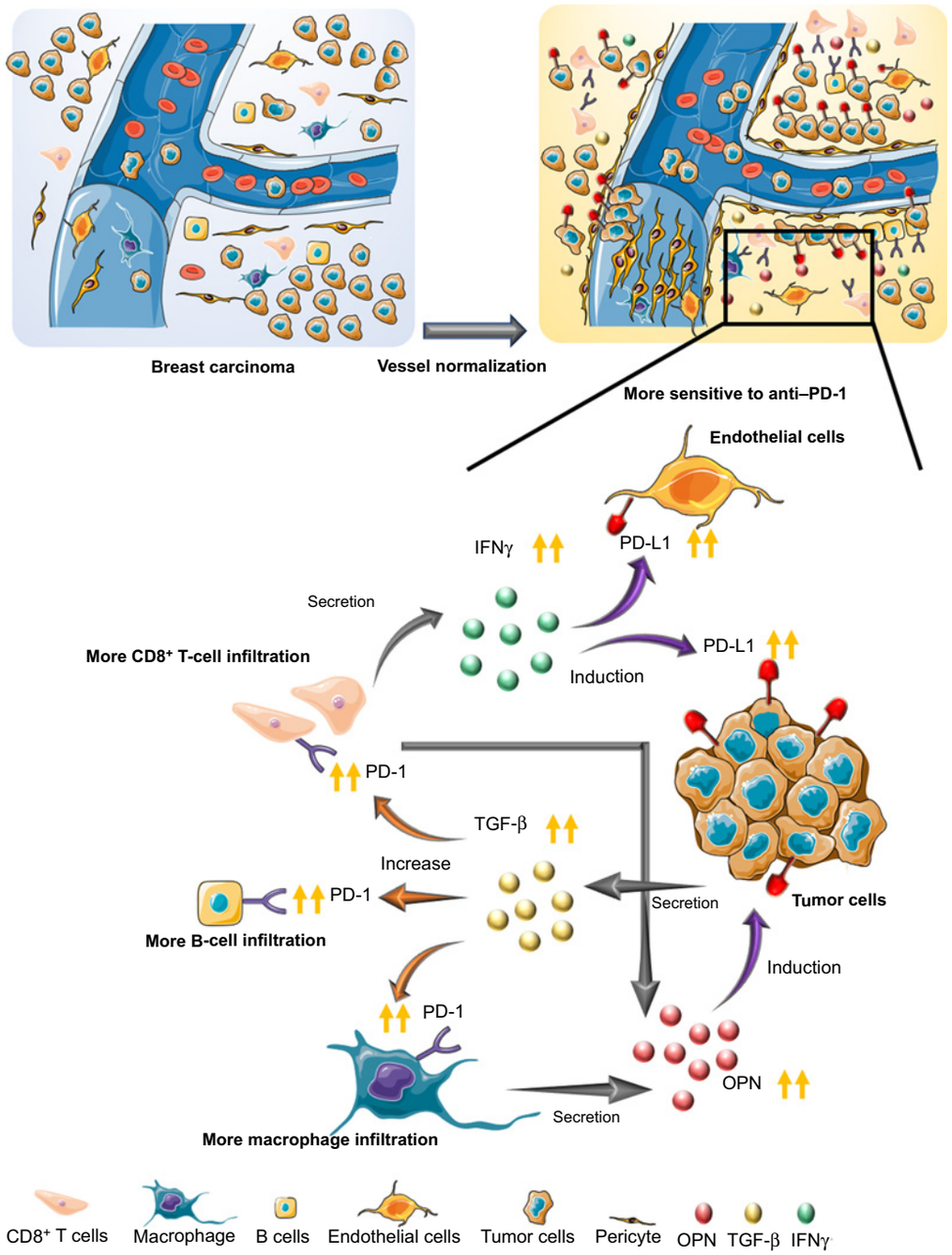

Figure 5.
An overview schematic demonstrating that low-dose anti-VEGFR2 antibody modifies the tumor microenvironment and potentiates the antitumor effect of anti–PD-1 immune therapy.

progression-free survival (PFS) for these 12 patients was 3.7 months [95% confidence interval (CI), 1.7–not reached], which was more favorable than for similar patients enrolled in the phase Ib KEYNOTE-012 trial who received single-agent anti–PD-1 antibody (median PFS, 1.9 months; 95% CI, 1.7–5.5; ref. 2). We then stratified all patients into good-responder and poor-responder groups according to the median PFS (**Fig. 6A**). For safety analysis, only one (8.3%) patient discontinued apatinib therapy, and two (16.7%) patients required apatinib dose reduction. The adverse effects (AE) of these 12 patients are summarized in **Fig. 6B**, and the majority of these AEs were mild and tolerable. We found that the vessel density exhibited minimal changes in tumors among patients in the poor-responders group after combination treatment. In contrast, notable vascular remodeling effects were observed in the good-responders group (**Fig. 6C**). We then

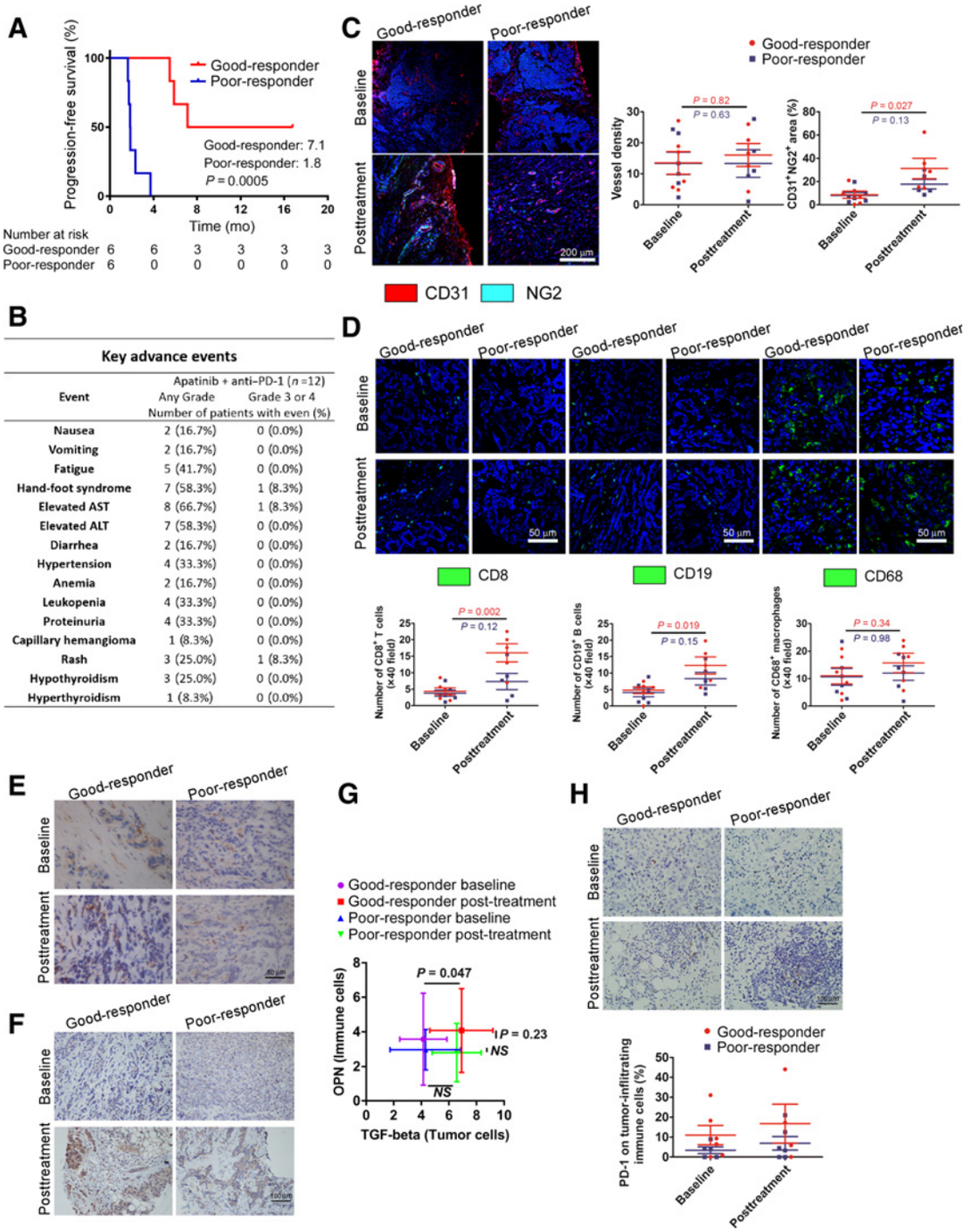

Figure 6.

Anti–PD-1 antibody and blood vessel normalization dose VEGFR2-TKI combination therapy showed favorable antitumor activities in patients with advanced TNBC. **A,** The Kaplan–Meier curves for PFS of patients in the good- and poor-responder groups. **B,** Key advance events of the enrolled patients. **C,** Vessel density and vascular normalization in patients with TNBC. Representative images of CD31 (red) and NG2 (cyan) immunostaining and DAPI nuclear staining (blue) of patients with TNBC who were less or more sensitive to treatment; scale bars, 200 μm. Each dot indicates one tumor per patient and represents the average of 5–8 images. **D,** Representative immunofluorescence staining of CD8, CD19, and CD68 in the serial sections of resected breast cancer samples collected from more and less sensitive patients before or after treatment; scale bar, 50 μm. Each dot indicates one tumor per patient and represents the average of 5–8 images. **E** and **F,** Representative immunohistochemistry (IHC) staining of OPN (**E**, scale bar 50 μm), and TGF-β1 (**F**, scale bar 100 μm) in breast cancer samples collected from responder and nonresponder patients before or after therapy. **G,** Correlation between OPN in immune cells and TGF-β in tumor cells. **H,** PD-1 in breast cancer samples collected from responder and nonresponder patients before or after therapy; scale bar, 100 μm. Data are presented as means ± SEM. *, $P < 0.05$; **, $P < 0.01$; ***, $P < 0.001$ by Student t test.

performed immune profiling of the tumor-infiltrated cells and found that good-responding tumors had more tumor-infiltrating $CD8^+$ T cells and B cells after treatment than poor-responders. The number of tumor-infiltrating macrophages also trended toward enhanced sensitivity to the therapy, although did not reach statistical significance (**Fig. 6D**).

Finally, we found that the tumors of good-responders had increased levels of immune cell-derived OPN and more tumor-derived TGF-β than those from poor-responders (**Fig. 6E–G**). PD-1 expression on infiltrated immune cells pre- and post-treatment was not correlated with patient response, maybe due to small sample size (**Fig. 6H**).

Discussion

In summary, we showed that combining anti–PD-1 antibody and low-dose anti-VEGFR2 therapy significantly improved antitumoral responses in preclinical models of breast carcinoma and exhibited encouraging therapeutic efficacy in patients with advanced TNBC. We showed that, although both full- and low-dose DC101 enhanced PD-L1 expression on tumor, endothelial, and immune cells, low-dose DC101 enhanced immune cell infiltration when combined with anti–PD-1. Furthermore, low-dose DC101 sensitized tumors to anti–PD-1 therapy via upregulation of PD-1 on immune cells through stimulating the secretion of OPN and TGF-β. These effects were absent when tumors were treated with full-dose DC101.

Our results suggest that OPN is a crucial factor in regulating the tumor immune microenvironment. Blocking OPN with a neutralizing antibody diminished the synergy of anti–PD-1 and low-dose DC101 combination therapy. In patients with advanced TNBC treated with low-dose VEGFR2 inhibitor apatinib and anti–PD-1 antibody SHR-1210, we found a correlation between clinical response and the expression of OPN and TGF-β following treatment. OPN is a bone matrix protein that plays several important roles in cell trafficking, cytokine production, and immune regulation (21). OPN has been reported to induce TGF-β expression in mesenchymal stem cells to promote transformation of cancer-associated fibroblasts (22). High expression levels of OPN may induce immunosuppression (23) and promote metastasis (24), and are associated with poor prognosis in multiple cancers (25). OPN is also involved in regulating angiogenesis, as it recruits proangiogenic monocytes to induce blood vessel formation (26). Crosstalk between OPN and VEGF has been reported, and prior studies have shown that OPN blockade inhibited angiogenesis more effectively than anti-VEGFR treatment (27–29). Our finding that anti-VEGFR2 treatment relies on the production of OPN to potentiate anti–PD-1 therapy reveals the intriguing functions of OPN and emphasizes the complexity of intratumoral immune signaling. However, the threshold for anti-angiogenic agents to induce OPN secretion and the biological mechanism underlying such stimulation are still unknown. In addition, the exact effects of OPN on tumor angiogenesis, immune regulation and on the potential responses of tumors to immune checkpoint blockades warrant further investigations.

Anti-angiogenic therapy has been used to treat multiple types of cancer for decades, but its efficacy is not favorable, and patient benefits are minimal (30). Anti-angiogenic therapies often induce severe side effects, including cardiovascular toxicities (31) and hemorrhaging (32). When treating patients with advanced TNBC, a previous multicenter phase II trial showed that the toxicity of apatinib depended on dosage. In the trial, 68% of patients in the 750 mg/d-dose group required dose reduction or dose interruption, whereas in the 500 mg/d-dose group, 25.4% of patients discontinued apatinib therapy, and 32.2% of patients had their dose reduced; so, the recommended dose was 500 mg/d, with a relatively low ORR of 10.7% (33). In our study with low-dose apatinib plus anti–PD-1 combination therapy, only one patient (8.3%) discontinued apatinib therapy, and two patients (16.7%) required dose reduction, suggesting that the combination therapy was well tolerated. Therapeutically, conventional anti-angiogenic therapy is intended to eradicate tumor vasculatures (17). However, excessively inhibiting tumor blood vessel formation reduces vessel perfusion, which impedes immune cell infiltration and drug delivery (5, 30). The hypoxia caused by vessel abnormality further induces resistance to other therapies and creates an immunosuppressive microenvironment (5). Nevertheless, studies in recent years have demonstrated that tumor vasculature plays critical roles in the tumor immune microenvironment and that the key to successful anti-angiogenic therapy is to control the dose to a vessel-normalizing level (13, 17). Huang and colleagues (13) showed that a vascular normalizing dose of anti-VEGFR2 antibody increased T lymphocyte infiltration and induced tumor-associated macrophages to polarize toward an immune-stimulatory M1 phenotype. Targeting tumor blood vessels by genetic knockout of Rgs5 (34) or anti-angiogenic agents that inhibited VEGFR or bio-specifically targeted ANGPT2 and VEGFA (11, 12) enhanced the efficacy of immunotherapies. In addition, immunotherapy may also exert vascular normalizing effects (35–38). The reciprocal effects of anti-angiogenic therapy and immunotherapy makes combining these two modalities a promising novel treatment combination that warrants further investigation in both preclinical and clinical settings.

Although we observed a trend associating high TGF-β and OPN levels with better response in patients, the differences between the two groups have not reached statistical significance, likely due to the small number of enrolled patients. The trial data showed that the good responders had more $CD8^+$ T-cell infiltration post-treatment, which might be either the result of better vessel normalization, or the reason for better immunotherapy response. Because T cells have been reported to normalize tumor vasculatures (35, 36), it is possible that both anti-angiogenetic agents and the checkpoint blockades contributed to the modification of the tumor microenvironment. The phase II study here is not a randomized controlled trial comparing anti–PD-1 monotherapy and anti–PD-1 combined with apatinib; although we showed that low-dose apatinib or DC101 combined with anti–PD-1 had better antitumor efficacy than anti–PD-1 alone in several animal models, the exact role of anti-angiogenic agents in this combination with anti–PD-1 antibody for patients with breast cancer needs further investigation. In addition, the post-treatment biopsy was performed 8 weeks after the treatment concluded; some immediate changes in the tumor microenvironment may not have been captured at this time point.

As we demonstrated that high-dose is less effective than low-dose DC101 in combination with PD-1 blockade, personalizing anti-angiogenic agents for each patient will be the most important issue and the foremost challenge to clinical application. Determining the optimal dosing regimen for individual patients could be challenging, because several conditions affect anti-angiogenic therapy, such as VEGF polymorphisms (39), circulating angiogenic molecules (39), and the tumor microenvironment (40). One possible solution to overcome this limitation is to closely monitor tumor vascular changes during the course of the treatment using non-invasive methods. Recent studies have shown that immune checkpoint blockade can improve

tumor vessel perfusion, which was associated with antitumor responses (35). These non-invasive strategies provide real-time feedback for clinicians to adjust the dose of anti-angiogenic agents and should be tested in future clinical trials.

In conclusion, our study demonstrated the dose-dependent synergy of anti-angiogenic therapy and an anti–PD-1 antibody in preclinical breast cancer models and in patients with advanced TNBC. These results further highlight the importance of dose considerations for anti-angiogenic therapy when combining with immune checkpoint blockade and provide a new rationale for advancing this combination therapeutic strategy in the clinic.

Disclosure of Potential Conflicts of Interest

No potential conflicts of interest were disclosed.

Authors' Contributions

Conception and design: Y. Wang, W. Jiang, Q. Liu, J. Liu
Development of methodology: J. Liu
Acquisition of data (provided animals, acquired and managed patients, provided facilities, etc.): Q. Li, W. Jia, J. Chen, J. Liu
Analysis and interpretation of data (e.g., statistical analysis, biostatistics, computational analysis): Q. Li, Y. Wang, H. Deng, G. Li, W. Deng, B.Y.S. Kim, W. Jiang, J. Liu
Writing, review, and/or revision of the manuscript: Q. Li, Y. Wang, B.Y.S. Kim, W. Jiang, Q. Liu, J. Liu
Administrative, technical, or material support (i.e., reporting or organizing data, constructing databases): J. Liu
Study supervision: W. Jiang, J. Liu

Acknowledgments

This work was supported by grants from the National Natural Science Foundation of China (81602673; to J. Liu), the Cancer Prevention and Research Institute of Texas (RR180017; to W. Jiang), and the Susan G. Komen Foundation (CCR19605871; to W. Jiang).

The costs of publication of this article were defrayed in part by the payment of page charges. This article must therefore be hereby marked *advertisement* in accordance with 18 U.S.C. Section 1734 solely to indicate this fact.

Received July 8, 2019; revised November 3, 2019; accepted December 12, 2019; published first December 17, 2019.

References

1. Dirix LY, Takacs I, Jerusalem G, Nikolinakos P, Arkenau HT, Forero-Torres A, et al. Avelumab, an anti–PD-L1 antibody, in patients with locally advanced or metastatic breast cancer: a phase 1b JAVELIN solid tumor study. Breast Cancer Res Treat 2018;167:671–86.
2. Nanda R, Chow LQ, Dees EC, Berger R, Gupta S, Geva R, et al. Pembrolizumab in patients with advanced triple-negative breast cancer: phase Ib KEYNOTE-012 study. J Clin Oncol 2016;34:2460–7.
3. Emens LA, Cruz C, Eder JP, Braiteh F, Chung C, Tolaney SM, et al. Long-term clinical outcomes and biomarker analyses of atezolizumab therapy for patients with metastatic triple-negative breast cancer: a phase 1 study. JAMA Oncol 2019; 5:74–82.
4. Emens LA, Ascierto PA, Darcy PK, Demaria S, Eggermont AMM, Redmond WL, et al. Cancer immunotherapy: opportunities and challenges in the rapidly evolving clinical landscape. Eur J Cancer 2017;81:116–29.
5. Huang Y, Kim BYS, Chan CK, Hahn SM, Weissman IL, Jiang W. Improving immune-vascular crosstalk for cancer immunotherapy. Nat Rev Immunol 2018; 18:195–203.
6. Lanitis E, Irving M, Coukos G. Targeting the tumor vasculature to enhance T-cell activity. Curr Opin Immunol 2015;33:55–63.
7. Corzo CA, Condamine T, Lu L, Cotter MJ, Youn JI, Cheng P, et al. HIF-1alpha regulates function and differentiation of myeloid-derived suppressor cells in the tumor microenvironment. J Exp Med 2010;207:2439–53.
8. Facciabene A, Peng X, Hagemann IS, Balint K, Barchetti A, Wang LP, et al. Tumour hypoxia promotes tolerance and angiogenesis via CCL28 and T(reg) cells. Nature 2011;475:226–30.
9. Barsoum IB, Smallwood CA, Siemens DR, Graham CH. A mechanism of hypoxia-mediated escape from adaptive immunity in cancer cells. Cancer Res 2014;74:665–74.
10. Koh J, Jang JY, Keam B, Kim S, Kim MY, Go H, et al. EML4-ALK enhances programmed cell death-ligand 1 expression in pulmonary adenocarcinoma via hypoxia-inducible factor (HIF)-1alpha and STAT3. Oncoimmunology 2016;5: e1108514.
11. Allen E, Jabouille A, Rivera LB, Lodewijckx I, Missiaen R, Steri V, et al. Combined antiangiogenic and anti–PD-L1 therapy stimulates tumor immunity through HEV formation. Sci Transl Med 2017;9:pii:eaak9679.
12. Schmittnaegel M, Rigamonti N, Kadioglu E, Cassara A, Wyser Rmili C, Kiialainen A, et al. Dual angiopoietin-2 and VEGFA inhibition elicits antitumor immunity that is enhanced by PD-1 checkpoint blockade. Sci Transl Med 2017;9:pii:eaak9670.
13. Huang Y, Yuan J, Righi E, Kamoun WS, Ancukiewicz M, Nezivar J, et al. Vascular normalizing doses of antiangiogenic treatment reprogram the immunosuppressive tumor microenvironment and enhance immunotherapy. Proc Natl Acad Sci U S A 2012;109:17561–6.
14. Lee SJ, Lee SY, Lee WS, Yoo JS, Sun JM, Lee J, et al. Phase I trial and pharmacokinetic study of tanibirumab, a fully human monoclonal antibody to vascular endothelial growth factor receptor 2, in patients with refractory solid tumors. Invest New Drugs 2017;35:782–90.
15. Willett CG, Boucher Y, Duda DG, di Tomaso E, Munn LL, Tong RT, et al. Surrogate markers for antiangiogenic therapy and dose-limiting toxicities for bevacizumab with radiation and chemotherapy: continued experience of a phase I trial in rectal cancer patients. J Clin Oncol 2005; 23:8136–9.
16. Rimm DL, Han G, Taube JM, Yi ES, Bridge JA, Flieder DB, et al. A Prospective, multi-institutional, pathologist-based assessment of 4 immunohistochemistry assays for PD-L1 expression in non–small cell lung cancer. JAMA Oncol 2017;3: 1051–8.
17. Huang Y, Goel S, Duda DG, Fukumura D, Jain RK. Vascular normalization as an emerging strategy to enhance cancer immunotherapy. Cancer Res 2013;73: 2943–8.
18. Thommen DS, Koelzer VH, Herzig P, Roller A, Trefny M, Dimeloe S, et al. A transcriptionally and functionally distinct PD-1(+) CD8(+) T cell pool with predictive potential in non–small cell lung cancer treated with PD-1 blockade. Nat Med 2018;24:994–1004.
19. Tumeh PC, Harview CL, Yearley JH, Shintaku IP, Taylor EJ, Robert L, et al. PD-1 blockade induces responses by inhibiting adaptive immune resistance. Nature 2014;515:568–71.
20. Pare L, Pascual T, Segui E, Teixido C, Gonzalez-Cao M, Galvan P, et al. Association between PD1 mRNA and response to anti-PD1 monotherapy across multiple cancer types. Ann Oncol 2018;29:2121–8.
21. Zhao H, Chen Q, Alam A, Cui J, Suen KC, Soo AP, et al. The role of osteopontin in the progression of solid organ tumour. Cell Death Dis 2018;9:356.
22. Weber CE, Kothari AN, Wai PY, Li NY, Driver J, Zapf MA, et al. Osteopontin mediates an MZF1-TGF-beta1-dependent transformation of mesenchymal stem cells into cancer-associated fibroblasts in breast cancer. Oncogene 2015; 34:4821–33.
23. Klement JD, Paschall AV, Redd PS, Ibrahim ML, Lu C, Yang D, et al. An osteopontin/CD44 immune checkpoint controls $CD8^+$ T-cell activation and tumor immune evasion. J Clin Invest 2018;128:5549–60.
24. Li NY, Weber CE, Mi Z, Wai PY, Cuevas BD, Kuo PC. Osteopontin upregulates critical epithelial–mesenchymal transition transcription factors to induce an aggressive breast cancer phenotype. J Am Coll Surg 2013;217:17–26.
25. Weber GF, Lett GS, Haubein NC. Osteopontin is a marker for cancer aggressiveness and patient survival. Br J Cancer 2010;103:861–9.
26. Leali D, Dell'Era P, Stabile H, Sennino B, Chambers AF, Naldini A, et al. Osteopontin (Eta-1) and fibroblast growth factor-2 cross-talk in angiogenesis. J Immunol 2003;171:1085–93.

27. Chakraborty G, Jain S, Kundu GC. Osteopontin promotes vascular endothelial growth factor-dependent breast tumor growth and angiogenesis via autocrine and paracrine mechanisms. Cancer Res 2008;68: 152–61.
28. Ramchandani D, Weber GF. Interactions between osteopontin and vascular endothelial growth factor: implications for cancer. Biochim Biophys Acta 2015; 1855:202–22.
29. Dai J, Peng L, Fan K, Wang H, Wei R, Ji G, et al. Osteopontin induces angiogenesis through activation of PI3K/AKT and ERK1/2 in endothelial cells. Oncogene 2009;28:3412–22.
30. Jain RK. Antiangiogenesis strategies revisited: from starving tumors to alleviating hypoxia. Cancer Cell 2014;26:605–22.
31. des Guetz G, Uzzan B, Chouahnia K, Morere JF. Cardiovascular toxicity of anti-angiogenic drugs. Target Oncol 2011;6:197–202.
32. Elice F, Rodeghiero F. Side effects of anti-angiogenic drugs. Thromb Res 2012; 129(Suppl 1):S50–3.
33. Hu X, Zhang J, Xu B, Jiang Z, Ragaz J, Tong Z, et al. Multicenter phase II study of apatinib, a novel VEGFR inhibitor in heavily pretreated patients with metastatic triple-negative breast cancer. Int J Cancer 2014;135:1961–9.
34. Hamzah J, Jugold M, Kiessling F, Rigby P, Manzur M, Marti HH, et al. Vascular normalization in Rgs5-deficient tumours promotes immune destruction. Nature 2008;453:410–4.
35. Zheng X, Fang Z, Liu X, Deng S, Zhou P, Wang X, et al. Increased vessel perfusion predicts the efficacy of immune checkpoint blockade. J Clin Invest 2018;128: 2104–15.
36. Tian L, Goldstein A, Wang H, Ching Lo H, Sun Kim I, Welte T, et al. Mutual regulation of tumour vessel normalization and immunostimulatory reprogramming. Nature 2017;544:250–4.
37. Wang Y, Liu ZG, Yuan H, Deng W, Li J, Huang Y, et al. The reciprocity between radiotherapy and cancer immunotherapy. Clin Cancer Res 2019;25:1709–17.
38. Liu Z, Wang Y, Huang Y, Kim BYS, Shan H, Wu D, et al. Tumor vasculatures: a new target for cancer immunotherapy. Trends Pharmacol Sci 2019;40:613–23.
39. Jain RK, Duda DG, Willett CG, Sahani DV, Zhu AX, Loeffler JS, et al. Biomarkers of response and resistance to antiangiogenic therapy. Nat Rev Clin Oncol 2009;6: 327–38.
40. Ma S, Pradeep S, Hu W, Zhang D, Coleman R, Sood A. The role of tumor microenvironment in resistance to anti-angiogenic therapy. F1000Res 2018; 7:326.